4-10-2008

The Nature of the Ultraluminous Oxygen-Rich Supernova Remnant in NGC 4449

Dan Milisavljevic
Dartmouth College

Robert A. Fesen
Dartmouth College

The Astrophysical Journal, 677:306–316, 2008 April 10

THE NATURE OF THE ULTRALUMINOUS OXYGEN-RICH SUPERNOVA REMNANT IN NGC 4449

Dan Milisavljevic and Robert A. Fesen
6127 Wilder Lab, Department of Physics and Astronomy, Dartmouth College, Hanover, NH 03755;
danmil@dartmouth.edu, fesen@snr.darmouth.edu
Received 2007 September 1; accepted 2007 December 8

ABSTRACT

Optical images and spectra, both ground based and taken by *Hubble Space Telescope* (*HST*), of the young, luminous O-rich supernova remnant in the irregular galaxy NGC 4449 are presented. *HST* images of the remnant and its local region were obtained with the ACS/WFC using filters F435W, F555W, F814W (*B*, *V*, and *I*, respectively), F502N ([O III]), F658N (Hα +[N II]), F660N ([N II]), and F550M (line-free continuum). These images show an unresolved remnant (FWHM $< 0.05''$) located within a rich cluster of OB stars which itself is enclosed by a nearly complete interstellar shell seen best in Hα + [N II] emission approximately $8'' \times 6''$ (150 pc $\times$ 110 pc) in size. The remnant and its associated OB cluster are isolated from two large nearby H II regions. The ACS [O III] image shows the remnant may be partially surrounded by a clumpy ring of emission approximately $1''$ ($\sim$20 pc) in diameter. Recent ground-based spectra of the remnant reveal (1) the emergence of broad, blueshifted emission lines of [S II] $\lambda\lambda$6716, 6731, [Ar III] λ7136, and [Ca II] $\lambda\lambda$7291, 7324 which were not observed in spectra taken in 1978–1980; (2) faint emission at 6540–6605 Å centered about Hα and [N II] $\lambda\lambda$6548, 6583 with an expansion velocity of 500 ± 100 km s^{-1}; and (3) excess emission around 4600–4700 Å suggestive of a Wolf-Rayet population in the remnant's star cluster. We use these new data to re-interpret the origin of the remnant's prolonged and bright luminosity and propose that the remnant is strongly interacting with dense, circumstellar wind loss material from a $\gtrsim$20 $M_\odot$ progenitor star.

Subject headings: circumstellar matter — stars: Wolf-Rayet — supernovae: general — supernova remnants

Online material: color figure

1. INTRODUCTION

NGC 4449 is a Magellanic irregular type galaxy located at an estimated distance of 3.82 ± 0.18 Mpc (Annibali et al. 2007). Situated in the northern outskirts of the galaxy, near two prominent H II regions, lies a young, oxygen-rich supernova remnant (SNR), hereafter SNR 4449-1. With an observed radio flux of 4 mJy at 4.8 GHz (2002 epoch; Lacey et al. 2007) and an X-ray luminosity of 2.4×10^{38} erg s^{-1} (Patnaude & Fesen 2003), the remnant ranks among the most luminous remnants known and is nearly an order of magnitude brighter than the most luminous SNR in our Galaxy, Cas A.

The SNR was first discovered in radio by Seaquist & Bignell (1978) as a bright, unresolved nonthermal radio source ($\sim$10 mJy at 2.7 GHz) approximately $1'$ north of the nucleus of the galaxy at a location nearly coincident with an H II region cataloged by Sabbadin & Bianchini (1979). Subsequent optical spectrophotometry showed two different types of line emissions: (1) narrow H II region-like lines, and (2) broad lines of forbidden oxygen attributable to a young SNR like Cas A (Balick & Heckman 1978).

Further studies in the optical, UV, and X-rays confirmed the SNR nature of the object and highlighted its unusual luminosity and relatively young age (Kirshner & Blair 1980; Blair et al. 1983, 1984). Optical spectra showed no broad hydrogen emission, yet very broad emission of [O I] $\lambda\lambda$6300, 6364, [O II] $\lambda\lambda$7320, 7330, and [O III] $\lambda\lambda$4959, 5007 suggestive of O-rich supernova (SN) ejecta with an expansion velocity of approximately 3500 km s^{-1} and emitting an observed flux greater than 3×10^{-13} erg s^{-1} cm^{-2}. Blair et al. (1983) concluded that the remnant was approximately 100–200 yr old and used several lines of reasoning to infer a massive progenitor star $\approx$25 $M_\odot$. Recent work in the X-ray has suggested an age as old as $\sim$380 yr (Summers et al. 2003).

The remnant appeared unresolved in ground-based optical images, and very long baseline interferometry (VLBI) measurements by de Bruyn (1983) gave an upper limit of the remnant's angular diameter of $\leq 0.07''$ (1.3 pc). A subsequent analysis of optical spectra taken in 1993 using the Faint Object Spectrograph (FOS) and images taken in 1996 with the Faint Object Camera (FOC) onboard the *Hubble Space Telescope* (*HST*) led Blair & Fesen (1998) to report expansion velocities of the remnant as high as 6000 km s^{-1} and place an upper limit of $0.028''$ on its diameter. This expansion velocity and size suggested an age around 100 yr.

While SNR 4449-1 is currently quite luminous, the significant decline in the remnant's X-ray and radio flux over the last three decades implies that it was even brighter in the past. Volger & Pietsch (1997), studying *ROSAT* PSPC and HRI detected X-ray sources in NGC 4449, found an X-ray (0.1–2.4 keV) luminosity of 4.7×10^{38} erg s^{-1}, a value approximately 50% of the value quoted by Blair et al. (1983) using data from the *Einstein X-ray Observatory* High-Resolution Imager. This apparent decline in emission agreed with more recent observations taken with the *Chandra X-ray Observatory*, which found $L_x = (2.4\text{–}4.0) \times 10^{38}$ erg s^{-1} (Patnaude & Fesen 2003; Summers et al. 2003). Similarly, a marked decline in emission at all radio frequencies has been observed with a drop of 13–4 mJy from 1973 to 2002 at 4.9 GHz (Lacey et al. 2007).

The underlying cause of SNR 4449-1's extraordinarily high luminosity has been proposed to be due to an especially strong interaction of the remnant with dense local interstellar and/or circumstellar material (ISM/CSM). Kirshner & Blair (1980) argued that the nature of the high luminosity could be best explained if the remnant was in fact embedded inside an H II region, and Blair et al. (1983) favored the scenario of the SNR expanding into an ordinary H II region ($n_0 \approx 25$ cm^{-3}) as opposed to a much denser ($n_0 \approx 150$ cm^{-3}) medium. Later observations of the object taken in the optical (Bowmans et al. 1997) have supported the general notion of strong interaction with an H II region.

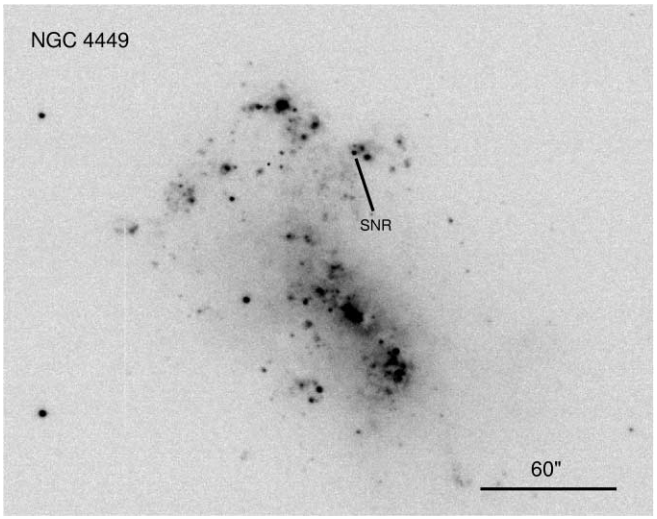

FIG. 1.— An [O III] λ5007 image of NGC 4449 obtained in 1996 showing the location of the young, O-rich supernova remnant 1′ north of the galaxy center. North is up and east is to the left.

Here we present optical ground-based and *HST* images and spectra that suggest the remnant may be interacting, not with an H II region, but rather with dense circumstellar material from a massive progenitor star. In § 2 we describe observations of the object with results from the images and spectra presented in § 3. We then discuss the nature of SNR 4449-1's high luminosity, describe its optical evolution, and compare it with other remnants and late-time SNe observations in § 4.

2. OBSERVATIONS

2.1. *Images*

A 200 s exposure of NGC 4449 was taken at MDM Observatory on 1996 May 21 with the 1.3 m McGraw-Hill telescope on Kitt Peak and a 2048×2048 pixel CCD with a plate scale of $0.44''$ pixel^{-1} yielding a $14.9' \times 14.9'$ field of view. A portion of this image is shown in Figure 1. A filter centered at $\lambda = 5000$ Å (FWHM = 110 Å) was used to detect SNR 4449-1's strong [O III] $\lambda\lambda$4959, 5007 line emission and place the remnant in context to neighboring H II regions.

High-resolution images of NGC 4449 were recently obtained by the Advanced Camera for Surveys (ACS; Ford et al. 1998; Pavlovsky et al. 2004) system on board *HST* using the Wide Field Channel (WFC), some of which covered the SNR 4449-1 region. A portion of some of these images were kindly made available before their public release by D. Calzetti (2007, private communication), with the rest retrieved from the STScI archives. The ACS/WFC consists of two 2048×4096 pixel CCDs providing a $202'' \times 202''$ field of view with an average pixel size of $0.05''$. Standard pipeline IRAF/STSDAS data reduction was done including debiasing, flat-fielding, geometric distortion corrections, photometric calibrations, and cosmic-ray and hot pixel removal, and the STSDAS `drizzle` task was used to combine exposures in each filter.

Table 1 lists ACS images of NGC 4449 that covered the O-rich SNR and were examined. The F502N filter is sensitive to the [O III] $\lambda\lambda$4959, 5007 lines, whereas F550M is a line-free continuum filter. The F658N filter passes both Hα λ6563 and [N II] $\lambda\lambda$6548, 6583 emission lines, while F660N isolates the [N II] λ6583 emission line. The broadband filters F435W, F555W, and F814W are equivalent to Johnson *B*, *V*, and *I* filters, respectively.

We used the ACS module of the DOLPHOT software (Dolphin 2000) to obtain photometry on these images. DOLPHOT is a point-spread function fitting package specifically tailored to do photometry of *HST* images. Photometry was done on the flat-fielded images from the STScI archive using the drizzled F435W as the reference image. The package identifies the sources and performs the photometry on individual frames, also taking into account all the information about image cosmetics and cosmic-ray hits that is attached to the observational material. DOLPHOT provides magnitudes corrected for charge-transfer efficiency effects on the calibrated VEGAMAG scale described by Sirianni et al. (2005). The package yields a variety of information for each object detected, including the object type (stellar, extended, etc.), χ^2 of the point-spread function fit, sharpness and roundness of the object, as well as a "crowding" parameter that measures how much brighter an object would have been had neighboring objects not been fit simultaneously. We selected objects of stellar type, valid photometry, $\chi^2 < 5$, and sharpness between -0.35 and $+0.35$.

TABLE 1
SUMMARY OF *HST* ACS/WFC IMAGES

Filter	λ_{cen} (Å)	λ_{FWHM} (Å)	Date (UT)	Exposure Time (s)
F435W.....	4297	1038	10 Nov 2005	3660
F502N	5022	57	18 Nov 2005	1284
F550M.....	5580	547	18 Nov 2005	1200
F555W.....	5346	1193	10 Nov 2005	2460
F658N	6560	73	17 Nov 2005	1539
F660N	6602	35	18 Nov 2005	1860
F814W.....	8333	2511	10 Nov 2005	2060

We also retrieved from the STScI archives high-resolution images of the remnant taken on 1996 February 22 by the Faint Object Camera previously on board the *HST*. The images have a field of view of $7.3'' \times 7.3''$ (512×512 pixels, with each pixel $0.014'' \times 0.014''$ in size). One image of exposure length 1635 s was taken with the F501N filter sensitive to [O III] ($\lambda_c = 5010$ Å; FWHM = 74 Å), and another of exposure length 596 s taken with the medium band F346M filter ($\lambda_c = 3480$ Å; FWHM = 434 Å). These COSTAR-corrected images were reduced in the standard STScI routine science data pipeline that performed flat-fielding and geometric corrections.

2.2. *Spectra*

Low-dispersion, optical spectra of SNR 4449-1 were obtained at MDM Observatory on Kitt Peak using the 2.4 m Hiltner telescope with a Modular Spectrograph and 2048×2048 pixel SITe CCD detector. Spectra were taken on 2002 June 17 and 2006 June 19 with total integration times of 2160 and 2700 s, respectively. Seeing was around $1''$ (FWHM) for the 2002 spectra and $1.5''$–$2.0''$ in 2006. A N–S $1.0'' \times 5.0'$ slit and a 600 line mm^{-1} 5000 Å blaze grism was used to obtain exposures spanning the spectral region 4300–7500 Å with a resolution of 4 Å.

The remnant was observed again at MDM Observatory using the same telescope, CCD detector, and spectrograph on 2007 April 9–15. The 600 line mm^{-1} 5000 Å blaze grism was used but now centered at 4500 Å to improve sensitivity in the blue and expand our lower spectral range to 4000 Å. We also used an 830 line mm^{-1} 8465 Å blaze grism centered around 7000 Å for a spectral region spanning 6100–8500 Å and a resolution of 3 Å. All spectra were reduced using standard IRAF[1] routines and calibrated with Hg, Ne, and Xe lamps and standard stars.

[1] The Image Reduction and Analysis Facility is distributed by the National Optical Astronomy Observatories, which are operated by the Association of Universities for Research in Astronomy, Inc., under cooperative agreement with the National Science Foundation.

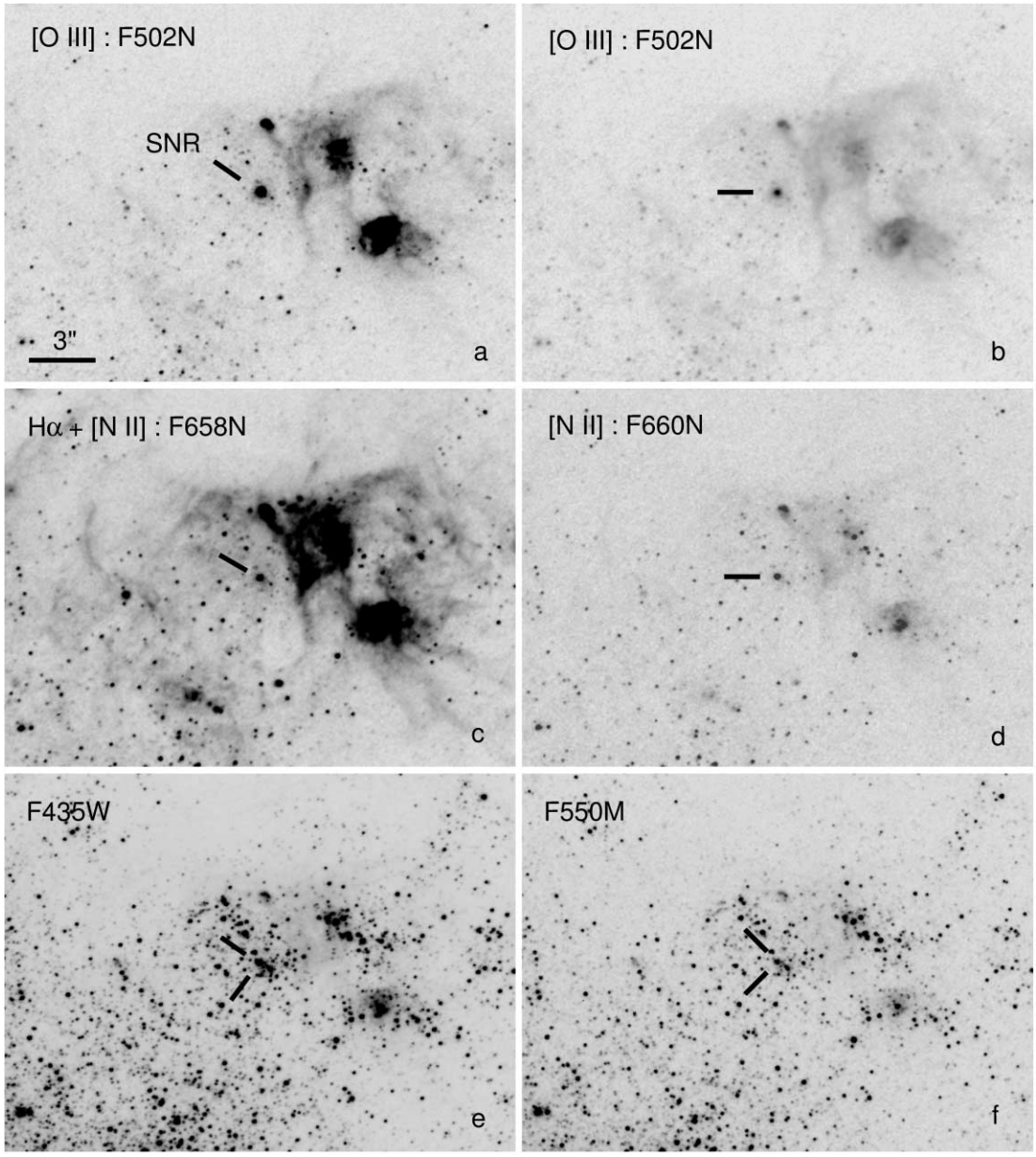

FIG. 2.—*HST* ACS/WFC images of the region surrounding SNR 4449-1 taken in 2005. (*a*) [O III] $\lambda\lambda$4959, 5007 (F502N). (*b*) Same as in (*a*), but highlighting the brightest sources. (*c*) Hα + [N II] (F658N). (*d*) [N II] λ6583 (F660N). (*e*) Blue (F435W). (*f*) Line-free continuum (F550M). North is up and east is to the left.

Archival optical spectra of the remnant taken with the FOS aboard the *HST* were also retrieved from STScI and examined (see Blair 1996). These spectra were taken on 1993 January 28 (pre-COSTAR correction) using a circular 1″ diameter aperture in combination with two gratings: (1) the G400H in FOS/RD configuration yielding spectral range 3400–4600 Å with resolution 4.0 Å, and (2) the G570H in FOS/RD configuration with spectral range 4800–6600 Å and resolution 5.9 Å. The total exposure time was 1250 s for each spectrum. The quality comment states that target acquisition failed during the pointing, so precise placement of the remnant inside the aperture is uncertain. Data were processed through standard FOS pipeline calibration, which includes detector background and scattered light subtraction, flat-field corrections, computation of wavelengths, and conversion from count rates to fluxes.

Measurements of observed flux reported from the spectra and photometry are corrected for extinction with $A_V = 0.7$ mag found from the Hα/Hβ ratio of our spectra. Reddening corrections were applied using this value and following the Cardelli et al. (1989) reddening law with $R_V = 3.1$.

3. RESULTS

3.1. *Environment around the SNR*

The high-resolution ACS/WFC images covering the SNR 4449-1 region provide the first clear look at its stellar and circumstellar environment (see Fig. 2). In the F502N [O III] image (Fig. 2*a*), one sees that the remnant is situated well to the east of two bright H II regions. A high-contrast version of this image, covering the same region, is shown in Figure 2*b*, illustrating that the remnant is by far the brightest unresolved source in this area at 5000 Å. The presence of a small possible faint [O III] emission ring surrounding the remnant will be discussed below in § 3.3.

The ACS/WFC Hα-sensitive F658N image presented in Figure 2*c* places the remnant most clearly in context with respect to the local H II regions. Previous ground-based observations suggested

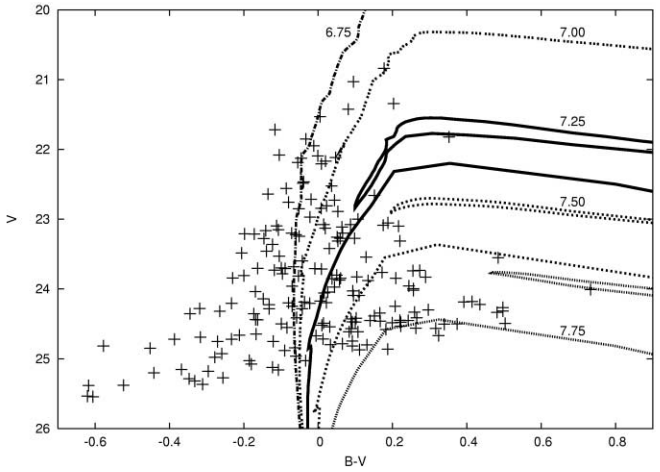

FIG. 3.—Color-magnitude diagram of the stars in the immediate projected vicinity of SNR 4449-1. Overlaid are isochrones of metallicity $Z = 0.004$ shifted to the distance, extinction, and reddening of the remnant. The estimated minimum age of the stellar population is $\log(\text{age yr}^{-1}) = 7.25 \pm 0.50$, consistent with the expected lifetime for stars with $M_{\rm ZAMS} = 15$–$25\ M_{\odot}$. [*See the electronic edition of the Journal for a color version of this figure.*]

that the remnant lay in or at the edge of the H II regions located immediately to the west (e.g., Bowmans et al. 1997). However, the high-resolution *HST* image shows that the remnant lies well away from the strong Hα emission associated with these regions. The image further reveals that the SNR is situated inside the cavity of an irregularly shaped emission shell approximately $8'' \times 6''$ (150 pc $\times$ 110 pc) in size. This shell is only weakly visible in [O III] (Fig. 2*a*) and barely noticeable in the [N II] (F660N) filter (Fig. 2*d*).

The location of SNR 4449-1 and the large Hα shell with respect to the local stellar environment is shown in Figure 2*e* and Figure 2*f* via the F435W and F550M continuum images. These images reveal that the remnant is situated inside a cluster of blue stars approximately $3'' \times 4''$ in size, all of which lies within the emission shell seen in the Hα + [N II] (F658N) image.

Photometry of this stellar cluster near SNR 4449-1 was conducted using the F435W, F555W, and F814W images. Only stars that were observed to be projected inside the Hα + [N II] emission shell and within approximately $3''$ of the remnant were measured. Figure 3 is a color-magnitude diagram of the resulting photometry, overlain with isochrones shifted to the distance, extinction, and reddening of the remnant to determine the most likely age of the cluster. The Geneva Group nonrotating stellar evolution models of Charbonnel et al. (1993) are shown with metallicity $Z = 0.004$ to best match the estimate of $Z = 0.005$ for NGC 4449 made by Annibali et al. (2007).

Following Massey et al. (2000) we assume that the stars of this association evolve in coeval fashion and use the turnoff mass of the cluster to make an estimate of the mass of the progenitor star of the remnant. As gauged by the cutoff of the youngest stars in the cluster, the lower limit of the age of the stellar population is approximately $\log(\text{age yr}^{-1}) = 7.25 \pm 0.50$. This is an age consistent with the expected lifetime of stars with $M_{\rm ZAMS} \simeq 15$–$25\ M_{\odot}$.

3.2. *The SNR*

The O-rich SNR is bright and unresolved in all of the narrowband *HST* images. The FWHM size of the remnant in the [O III] (F502N), Hα + [N II] (F658N), and [N II] (F660N) images is approximately 2.3 pixels ($0.12''$), comparable to the FWHM of stars on the images. The remnant has apparent magnitudes of $m_{\rm F502N} = 16.274 \pm 0.002$, $m_{\rm F658N} = 18.371 \pm 0.005$, and $m_{\rm F660N} = 18.435 \pm 0.008$. Previous spectra found little indication of any hydrogen and nitrogen emissions originating from the remnant (e.g., Kirshner & Blair 1980; Blair et al. 1983), so we found it surprisingly bright in the Hα + [N II] and [N II] λ6583 images.

To distinguish between Hα and [N II] λ6583 emissions from the remnant, we followed the absolute calibration for the F550M, F658N, and F660N filters outlined by O'Dell (2004). The F658N filter is nearly equally as good at transmitting both the Hα and stronger [N II] λ6583 lines, and the calibration procedure provides equations to separate their individual emission line fluxes. Using the count rates obtained with the DOLPHOT software and correcting the calibration constants of the F658N and F660N filters for the radial velocity 207 km s^{-1} of NGC 4449 (Schneider et al. 1992), we estimate a [N II] λ6583/Hα ratio of $\approx$1.

Bright, continuous emission at the location of the remnant is also observed in all of the wide-band ACS/WFC images in the F435W, F555W, and F814W filters. While these filters are sensitive to various emission lines of the remnant, the F550M filter with a bandwidth range between 5200–6000 Å is not, making it only sensitive to stellar continuum. The DOLPHOT software identifies three overlapping sources at the precise location of the remnant in the F550M image: two sources to the northwest and southwest of the remnant with magnitudes $m_{\rm F550M} = 23.120 \pm 0.025$ and 23.390 ± 0.028, respectively, and another with magnitude $m_{\rm F550M} = 22.246 \pm 0.016$ almost coincident (see Figs. 4*a* and 4*b*). Using the SYNPHOT package and the Bruzual Spectrum Synthesis Atlas to simulate the expected count rate from a stellar source, the entire flux within a $0.4''$ aperture around the center of emission containing all three sources in the F550M image is equivalent to approximately five O5 V stars ($\sim 3.4 \times 10^{-15}$ erg s^{-1} cm^{-2}).

Aligning the ACS/WFC images with the higher resolution FOC image adds clarity with respect to the three stellar sources identified by DOLPHOT at the remnant's location. Employing the `geomap` and `geotran` routines in IRAF, the FOC F346M image was aligned with the ACS/WFC F502N and F550M images (see Fig. 4*c*). While the alignment is prone to some uncertainty because of differences in scale and geometric distortion between the two instrument configurations, the placement of the remnant is quite clear. The SNR as defined by its [O III] emission coincides almost exactly with the brightest source of F346M emission, with smaller, less bright sources located to the northwest and southwest. These sources are labeled 1–3, respectively, in Figure 4*c*. Furthermore, the alignment shows that the locations of the three sources observed in the F346M image matches the arrangement of the continuum sources identified in the F550M image.

3.3. *A Circumstellar Ring?*

An apparent faint extended ring of emission situated immediately around the SNR, approximately $1''$ in diameter ($\sim$20 pc), is visible in the [O III] (F502N) image. To investigate the reality of this feature, the [O III] (F502N), Hα + [N II] (F658N), and [N II] λ6583 (F660N) images were continuum-subtracted using the line-free F550M image (see Fig. 5). As shown in this figure, the $1''$ ring is still weakly detected in [O III] after the subtraction, with a strength 0.3% of the peak flux of the remnant and $\sim$3 times above the background signal. The ring is not detected, however, in either Hα + [N II] or [N II] λ6583.

Initially, some properties of this apparent [O III] emission ring supported its authenticity. The ring structure appears clumpy and elliptical, features not normally associated with Airy diffraction rings or artifacts of filter reflections or scattering. However, a bright field star located approximately $45''$ east of the center of the galaxy in the F502N image was found to possess a ringlike structure sharing many similarities with that seen around SNR 4449-1. When overlaid with one another, the rings are of equal size

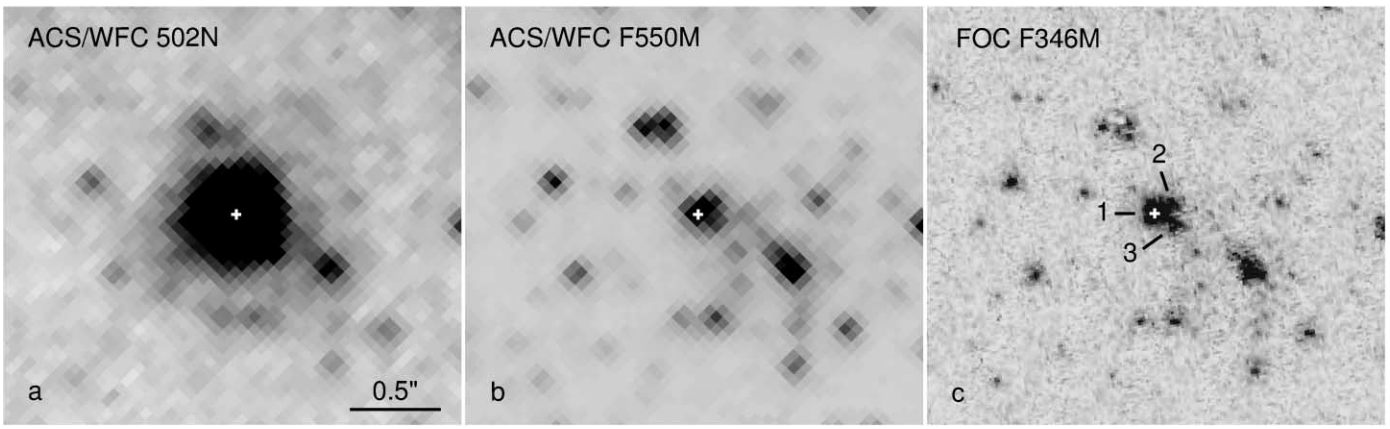

FIG. 4.—*HST* images of the stellar environment of SNR 4449-1. (*a*) ACS/WFC [O III] image with the plus sign marking the center of the remnant's emission. (*b*) ACS/WFC line-free continuum image with the plus sign marking the same location as the [O III] image. (*c*) High-resolution FOC F346M image. Note the location of the remnant coincides with a tight grouping of luminous stars. North is up and east is to the left.

(width $\approx 0.1''$) and have the same relative position from the center of emission. There is also a similar broken pattern in the encompassing ring, with a correspondence between the breaks in the ring of the field star and the apparent clumps in the thin ring around the remnant. Additional archival ACS/WFC images taken with the F502N filter were also retrieved to further investigate the nature of the [O III] ring, and we again found the same broken ring of equal size surrounding the brightest objects.

On the other hand, the correspondence between the ring features of the remnant and other bright sources is not perfect. Thin emission rings around bright field stars are perfectly round while the ring around SNR 4449-1 is noticeably elliptical with the major axis nearly north-south. Specifically, faint emission toward the north-northwest does not correspond to any features seen around field stars. Consequently, we conclude that much of the apparent [O III] emission ring seen in the F502N image is a diffraction ring, but with the possibility of some real [O III] emission surrounding the remnant, especially to the northwest.

3.4. *Optical Spectra*

3.4.1. *Temporal Change in Spectra*

A low-dispersion optical spectrum of the remnant taken in 2002 at MDM Observatory is presented in Figure 6. The spectrum shows the same two components previously observed by Kirshner & Blair (1980): (1) narrow lines of Hα, Hβ, [N II], and [S II] associated with H II region-like emission; and (2) broad lines of [O I], [O II], and [O III] associated with ejecta of a young, O-rich SNR. The forbidden oxygen expansion velocity $V_{\rm exp} \sim 6000$ km s^{-1}, measured from the half width at zero intensity from the [O III] λ5007 emission line toward the red, agrees with the value reported by Blair & Fesen (1998).

However, this 2002 spectrum also reveals emergent features not observed in the 1978–1980 optical spectra of the SNR taken by Kirshner & Blair (1980) and Blair et al. (1983). Broad, blueshifted emission lines with similar velocity profiles of Si-group elements [S II] $\lambda\lambda$6716, 6731, [Ar III] λ7136, and [Ca II] $\lambda\lambda$7291, 7324 are visible. Measured toward the blue and red of the [S II] $\lambda\lambda$6716 and 6731 lines, respectively, the velocities are estimated to lie in the range of $-2500 \leq V_{\rm exp} \leq 400$ km s^{-1}. The reduced and background-subtracted two-dimensional (2D) spectrum shown in Figure 7 illustrates the blueshifted [S II] and [Ar III] emission features more clearly than the one-dimensional (1D) spectrum presented in Figure 6. The [Ca II] emission, on the other hand, is difficult to see in both 1D and 2D spectra because it is blended with the strong [O II] $\lambda\lambda$7320, 7330 lines.

3.4.2. *Broad* Hα + [N II] *Emission*

Previous optical spectra noted a lack of hydrogen from the remnant (Kirshner & Blair 1980). However, our ground-based spectra reveal the presence of faint, broad emission extending from

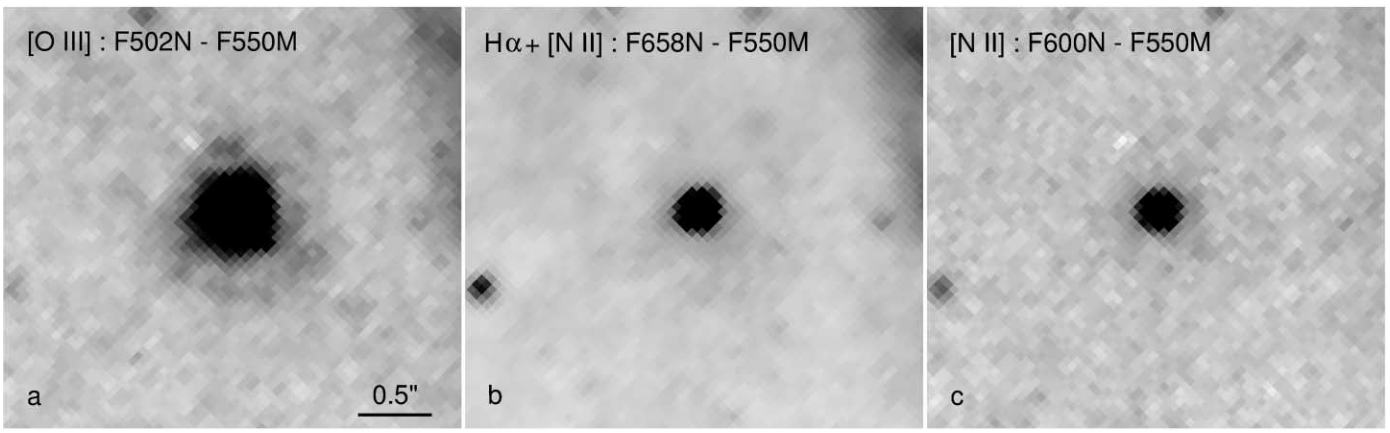

FIG. 5.—Enlarged *HST* continuum-subtracted images of SNR 4449-1. (*a*) [O III]-sensitive F502N image subtracted with a flux-calibrated and aligned F550M image. (*b*) Hα + [N II]–sensitive F658N image subtracted the same as in (*a*). (*c*) [N II] 6583-sensitive F660N image subtracted the same as in (*a*).

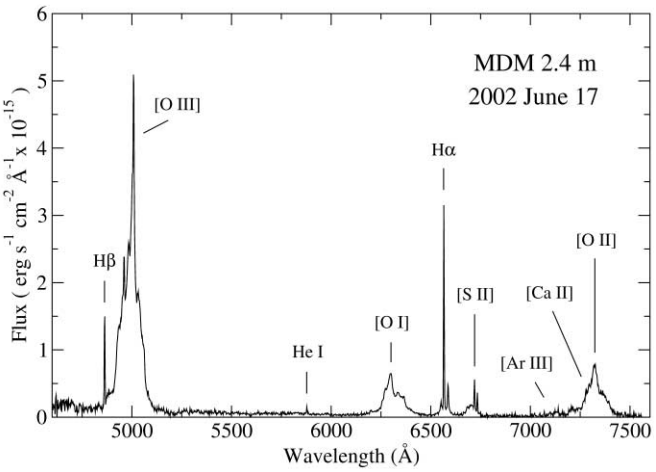

FIG. 6.—Spectrum of SNR 4449-1 taken with the MDM 2.4 m telescope.

around 6540 to 6605 Å centered near the narrow Hα line. Analysis of the raw spectrum suggests the observed extended emission is most likely the combination of slightly broadened [N II] $\lambda\lambda$6548, 6583 and Hα, each with velocities around 500 km s^{-1} (see Fig. 7).

Additional evidence for the presence of broad Hα emission comes from archival FOS spectra of the remnant, which we present in Figure 8. Our ground-based spectra in the optical lack the spatial resolution to completely isolate the remnant from the H II regions that lie less than 2″ away. The *HST* observations, however, make it possible to observe the remnant independent of the H II regions' strong emission lines that contaminate the spectra. This advantage makes the FOS spectra more sensitive to any faint Hα and [N II] emission that can be attributed to the remnant.

Similar to our ground-based observations, the FOS spectrum also shows an extended base in the region of Hα spanning 6540–6605 Å. The Hα and [N II] $\lambda\lambda$6548, 6583 lines are noticeably broad, so much so that the [N II] λ6548 emission line is barely discernible underneath the broad Hα. Deblending the lines, the profiles show $V_{\rm exp} = 500 \pm 100$ km s^{-1} for the [N II] and Hα lines, with the FWHM of the nitrogen lines appearing somewhat larger than Hα. The [N II] 6583/H$\alpha \approx 0.5$ ratio is slightly lower than our derived ratio from the ACS/WFC images, which is a discrepancy likely due to contamination from the surrounding diffuse H II emission (observed in the F658N image; see Fig. 2*c*) in the spectra that biases the Hα flux.

3.4.3. *Other Emission Lines*

In the near-UV of the FOS spectrum, the [Ne III] λ3869 and [O II] λ3727 lines have similar velocity profiles with a maximum expansion velocity of $\sim$5000 km s^{-1}. In Figure 9 we show the velocity line profiles of [O II] λ3727, [Ne III] λ3869, and [O III] $\lambda\lambda$4959, 5007 that have been smoothed with a five pixel boxcar function and scaled in arbitrary units of flux. The profiles share conspicuous emission peaks symmetrically spaced at approximately $\pm$1600 km s^{-1}. These minor emission peaks are present in both the *HST* FOS and ground-based spectra. Moreover, the emission profiles of [O I] $\lambda\lambda$6300, 6364 and [O II] $\lambda\lambda$7320, 7330 of the ground-based spectra share symmetric emission peaks around $\pm$1600 km s^{-1}. Interestingly, hints of minor emission peaks in the broad [S II] and [Ar III] lines are also observed at $-$1600 km s^{-1}.

The emission line profile of [O III] $\lambda\lambda$4959, 5007 seen in Figure 9 shows a staircase shape slightly skewed toward the blue. The peaks marked A and B correspond with emission from the lines at 4959 and 5007 Å, respectively. We interpret the adjacent emission peaks marked A_b and A_r as [O III] λ5007 emission blueshifted and redshifted by $\pm$1600 km s^{-1}. Likewise, we interpret the minor emission peaks marked B_b and B_r as [O III] λ4959 emission similarly blueshifted and redshifted. The overlap between the $\lambda\lambda$4959 and 5007 emission lines heightens the blue side of the profile.

Hints of two minor emission peaks at +3000 and +4600 km s^{-1} are also seen in the [O III] profile of the FOS spectra. The ground-based 2002–2007 spectra show some faint evidence for these peaks as well. However, they do not correspond with any distinguishable emission observed within the [O II] or [Ne III] lines. We compared the [O III] $\lambda\lambda$4959, 5007 emission peaks at +3000 and +4600 km s^{-1} of the FOS spectra with the [O I] $\lambda\lambda$6300, 6364 and [O II] $\lambda\lambda$7320, 7330 lines of the ground-based spectra and did not find significant similarity.

Additional faint emission in the form of a clump is observed in the forbidden oxygen lines of the ground-based spectra at velocities between $-$3000 and $-$6000 km s^{-1}. In Figure 7 we highlight an example of this emission (marked O Clump), seen blueward of the [O II] λ7320 line with a minor peak around $-$4600 km s^{-1}. Similarly blueshifted and faint emission is observed in the [O III] λ4959 line where a noticeable bump in emission from the remnant merges into the Hβ line of the nearby H II region (see Fig. 6). Although the clump is less pronounced in the remnant's [O I] λ6300 line, there is a noticeable blueshifted ledge of emission beginning around $-$3000 km s^{-1} and extending out to $-$6000 km s^{-1}.

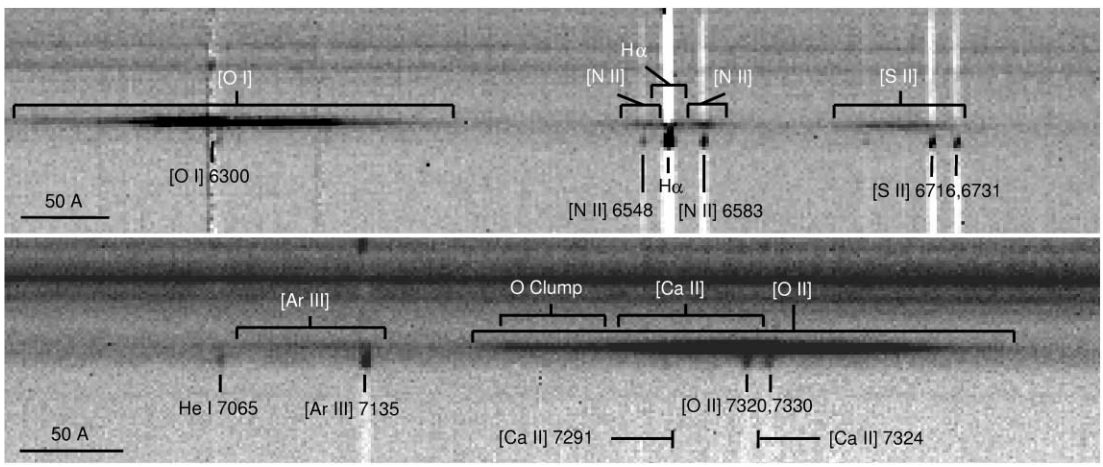

FIG. 7.—2D background-subtracted spectra of SNR 4449-1 taken with the MDM 2.4 m telescope. The top spectrum was taken in 2002 and the bottom spectrum was taken in 2007. Emission lines in the rest frame of the galaxy are marked in black, while the white labels highlight broad features.

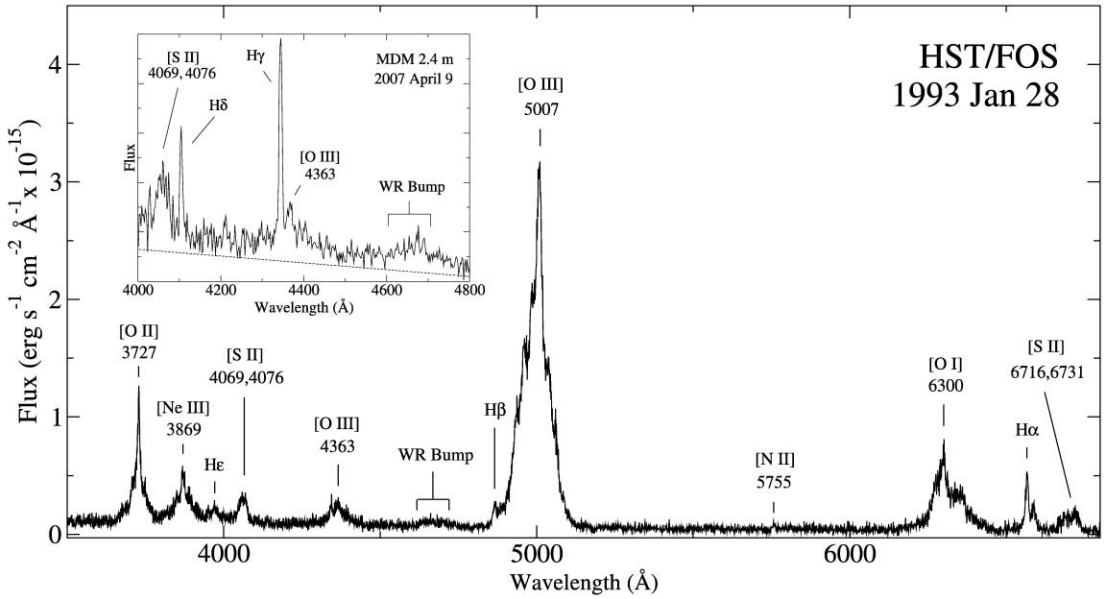

FIG. 8.—*HST* FOS spectrum of SNR 4449-1. The inset is a MDM spectrum that shares the WR-like broad emission at 4600–4700 Å.

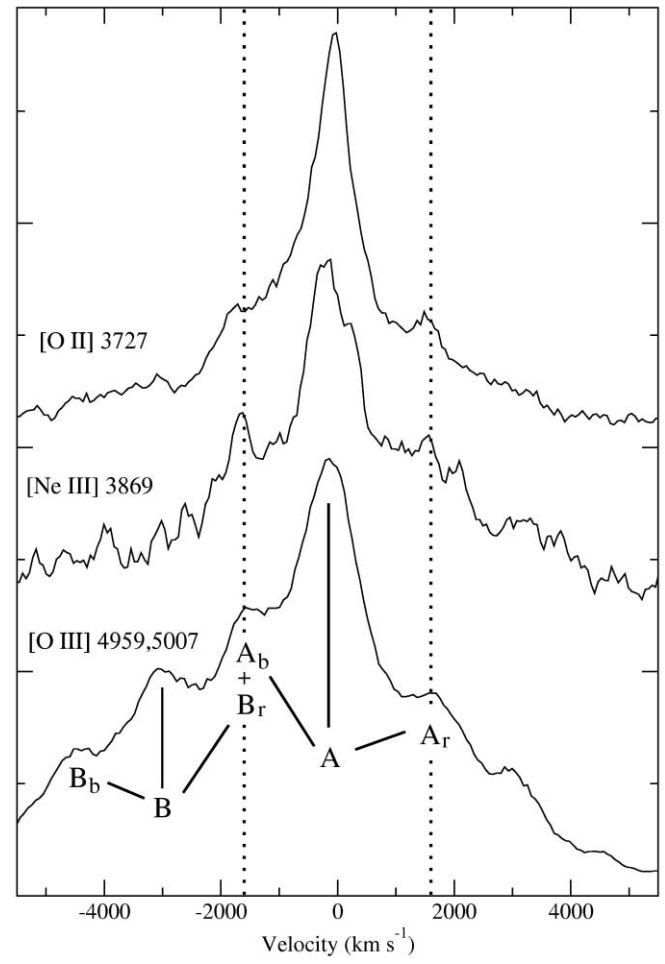

FIG. 9.—Smoothed velocity line profiles of [O II] λ3727, [Ne III] λ3869, and [O III] λλ4959, 5007 from *HST* FOS spectra obtained in 1993. Dotted lines are marked at ±1600 km s^{-1}. The [O III] profile is composed of the λ5007 line at 0 km s^{-1} (marked A) with associated blueshifted (A_b) and redshifted (A_r) emission, and the λ4959 line (marked B) with associated blueshifted (B_b) and redshifted (B_r) emission. Velocities are in the rest frame of NGC 4449.

The FOS spectra also weakly detects the temperature-sensitive emission line at [N II] λ5755. The relatively low [N II] λλ(6548+6583)/λ5755 $\lesssim$15 ratio implies unreasonably high temperatures of $\sim 10^5$ K for densities between 100–1000 cm^{-3}, so we suspect collisional de-excitation is quenching the [N II] λλ6548, 6583 lines. For this effect to be observed, electron densities greater than $\log n_e = 4.8$ are required. If we assume a temperature in the region of $T \sim 10^4$ K, the electron density is in the range $(1-1.5) \times 10^5$ cm^{-3}.

3.4.4. *A Wolf-Rayet Signature?*

In our ground-based spectra, a weak line is observed near 4689 Å that we suspect is He II λ4686, and it is coincident with broad, faint excess emission approximately 100 Å wide extending between 4600 and 4700 Å (see inset of Fig. 7). The detection of this feature is slight (S/N ~ 3), but its placement and shape is similar to a "WR bump" indicative of the presence of Wolf-Rayet (WR) stars at the location of the remnant. The FOS spectra show the same faint excess emission around the He II 4686 emission line, supporting our suspicion. Additional helium lines of He I at 5876, 6678, and 7065 Å are observed in the MDM spectra, but these originate from the nearby H II region and not from the remnant itself.

4. DISCUSSION

4.1. *Origin of SNR 4449-1's Extraordinary Brightness*

Young SNRs such as SNR 4449-1 are associated with two shocks likely to produce heating and observable radiation: (1) an outward-propagating blast wave running into surrounding material (CSM and/or ISM) giving rise to bright radio flux, and (2) an inward-propagating reverse shock that heats supernova ejecta and emits strongly across a wide spectral band. Previous studies of SNR 4449-1 attributed its high luminosity to a strong interaction between the remnant and a dense H II environment believed to encompass it (Kirshner & Blair 1980; Blair et al. 1983). However, the high-resolution ACS/WFC images clearly show the remnant isolated from the H II regions some 2″ away to the west (see Fig. 2*c*).

As assumed by previous analyses, we attribute the extremely broad ($V_{\rm exp} > 1000$ km s^{-1}) components of the spectra to interaction

between a reverse shock and the expanding O-rich debris. However, instead of the reverse shock originating from the blast wave running against an H II region ($n_e \approx 25$ cm^{-3}), the observations presented above strongly suggest that SNR 4449-1 is interacting with very dense and extensive circumstellar material. The intermediate velocity (500 ± 100 km s^{-1}) Hα and [N II] emissions likely originate from shock-heated CSM, and the high [N II] λ6583/Hα ratio $\approx$1 indicates it is N-rich. If we adopt the postshock density of $n_e \sim 10^5$ cm^{-3} implied by the [N II] λ5755 emission line and assume a temperature $T \sim 10^4$ K, the measured Hα flux of 1.0×10^{-14} erg s^{-1} cm^{-2} suggests a CSM mass of $\sim$0.5 $M_\odot$.

Alternatively, given that the remnant is coincident with bright stellar sources (see Fig. 4), it is also possible that UV emissions and/or interaction between the remnant and the stellar winds of nearby stars could contribute to the observed luminosity. The aligned FOC and ACS images show two stellar sources to the northwest and southwest of the remnant little more than 1 pc away, while the center of the relatively bright continuum source observed in the line-free (F550M) image lies within $\lesssim$0.3 pc of the center of the remnant as observed in the [O III] (F502N) image. In light of the high density inferred for the CSM, we view it as more likely that the continued brightness of SNR 4449-1 is the result of strong, ongoing interactions between the remnant and an extensive circumstellar environment left behind by its massive progenitor. However, the fact that the remnant is located within a compact stellar grouping less than a few parsecs in size allows for the possibility that it could also be interacting with the wind material of closely neighboring stars.

4.2. *The Progenitor Star*

If the assumption of coeval evolution is appropriate for the stellar cluster SNR 4449-1 is located in, the mass range of 15–25 $M_\odot$ derived from the photometry and stellar evolutionary tracks then represents a minimum mass for the progenitor. Our photometry and isochrone fitting agree with the results of Annibali et al. (2007), who used the same *HST* images but in combination with Padova stellar evolutionary tracks (Fagotto et al. 1994a, 1994b), and our mass estimate derived from the turnoff mass of the cluster is consistent with Blair et al. (1983), who argued for a progenitor star mass of $\sim$25 $M_\odot$ by comparing elemental abundances observed from optical and X-ray data with the stellar models of Weaver & Woosley (1980).

However, a 15–25 $M_\odot$ mass range is likely a modest estimate for the progenitor star. Because the remnant's emission lines extend across the wide passbands of the F435W, F555W, and F814W filters, we were unable to do photometry of the stars directly coincident with the remnant. Being located at the densest part of the cluster, these stars may represent the most massive members and, if so, could be of larger mass than the remainder we were able to do photometry on. Our mass estimate would also be larger if stars in this cluster are rotating. The low-metallicity models of Maeder & Meynet (2001) show that the lifetimes of massive rotating stars are longer than their nonrotating counterparts, meaning masses on rotating isochrones would be higher than the masses on nonrotating isochrones of the same age. Thus, the progenitor star of SNR 4449-1 could very well be greater than 20 $M_\odot$.

Excess broad emission around 4600–4700 Å near the He II λ4686 emission line (see Fig. 8) is a well-known feature of galaxies and clusters of stars harboring a significant population of Wolf-Rayet stars. Generally, this "WR bump" is a combination of many emission lines including N III $\lambda\lambda$4634, 4642, N V $\lambda\lambda$4605, 4622, and C III/C IV $\lambda\lambda$4650, 4658, in addition to He II λ4686. The presence of the WR bump in the spectra strongly suggests that WR stars are present near the location of the remnant, and the absence of carbon lines at C III λ5696 and C IV $\lambda\lambda$5801, 5812 suggests that most of the WR stars are of the WN type. Assuming that the progenitor star is among the most massive of the stars located here, the progenitor of SNR 4449-1 may have been a WR star itself.

On the other hand, the relatively broad profiles of Hα and [N II] with $V_{\rm exp} \approx 500$ km s^{-1}, along with the high density $\gtrsim 10^5$ cm^{-3} of the CSM implied by the [N II] λ5755 line, are not consistent with properties observed for WR stars and their circumstellar environments. WR stars are typically associated with wind velocities $\gtrsim$1000 km s^{-1}, and their nebulae generally have densities $<$1000 cm^{-3} (Esteban et al. 1992). Instead, these observations are more in line with properties found in luminous blue variables (LBVs) and their circumstellar nebulae. LBVs have slower wind velocities between 40 and 700 km s^{-1}, and higher densities in their circumstellar nebulae that, due to their clumpy nature, range between 10^3 and 10^7 cm^{-3} (Stahl 1989).

An LBV/WR progenitor star of SNR 4449-1 is an interesting possibility. However, such an implication is complicated by the inferred $\gtrsim$20 $M_\odot$ progenitor star mass which just meets the threshold for the mass of an O star to have mass loss substantial enough to strip away its outer atmosphere and develop into a WR star. Furthermore, LBVs are generally associated with stars of mass about 40 $M_\odot$ and greater. There are instances, however, where these evolved stars have been observed to lie in the 20 $M_\odot$ mass range. For example, the well-studied WR stars of the Ofpe/WN9 type along with their stellar and circumstellar environments share many of the characteristics observed around SNR 4449-1. These stars are observed to have similar mass ranges as derived from turnoff masses in stellar associations (Massey et al. 2000), are known to have a solid observational link with LBVs (Pasquali et al. 1997), and are frequently found in tight ($\lesssim$1 pc) groupings (Lortet 1989).

Aside from a single-star scenario, a progenitor with a binary companion is also a plausible way for a 20 $M_\odot$ star to evolve into a WR star, which in turn could lead to a SNe yielding an O-rich SNR. We note that low-metallicity environments such as NGC 4449 are understood to possess WR populations dominated by WR stars born in high-mass, close binary systems (Eldridge 2006). Furthermore, possible periodic variations in the overall downward decline in the radio flux of SNR 4449-1 (see Fig. 2 of Lacey et al. 2007) resemble the radio fluctuations observed in SN 1979C believed to most likely be consequence of interaction with a massive companion star in a highly eccentric orbit (Weiler et al. 1992). Thus, finding SNR 4449-1 in a tight grouping of luminous stellar sources makes binarity a strong possibility.

4.3. *SNR Evolution*

The optical spectra of SNR 4449-1 shows a number of emergent features when compared against spectra originally obtained in 1978–1980. The most obvious change that we observe is the development of broad, blueshifted emissions from [S II], [Ar III], and [Ca II]. The only previous evidence for broadening outside of forbidden oxygen was in the [S II] $\lambda\lambda$4069, 4076 lines, first observed by Balick & Heckman (1978) and later better resolved by Blair et al. (1983). Kirshner & Blair (1980) could find no evidence of broad [S II] $\lambda\lambda$6716, 6731 lines, making the presented spectra the first observation of broadening around these lines, and for all of the Si-group elements in general.

Evolution of the optical spectra of this sort was anticipated in previous studies (Balick & Heckman 1978; Seaquist & Bignell 1978; Kirshner & Blair 1980). The new line emission detections likely arise from the reverse-shock heating of a portion of SN ejecta (possibly a plume) of mixed O- and S-Ar-Ca-rich ejecta material.

Why these blueshifted emissions were not observed in previous spectra and are only observable now appears to be due in part to the continuing expansion of the ejecta, where the densities of the SN debris drop below the critical densities for collisional de-excitation of various S-Ar-Ca lines.

From an examination of the optical spectra of SNR 4449-1 in Blair et al. (1983) we estimate the broadening in the [S II] $\lambda\lambda$4069, 4076 emission lines to have FWZI $\approx$ 3500 km s^{-1}. This width corresponds to the broadening in the [S II] $\lambda\lambda$6716, 6731 lines measured in the 2002 spectra. The [S II] emission lines have a critical density of log $n_e \approx 3.4$, which is lower than the log $n_e \approx 6.4$ critical density of the [S II] $\lambda\lambda$4069, 4076 lines. Hence, it is a natural consequence for the red [S II] $\lambda\lambda$6716, 6731 lines to be visible following a decline in the density of the expanding shock-excited ejecta.

Finally, we note that minor emission peaks in the velocity profile of the forbidden oxygen lines of SNR 4449-1, first recognized by Kirshner & Blair (1980) and seen in our more recent spectra, suggest the presence of clumpy ejecta with a possible symmetry between facing and rear expanding hemispheres. The matching minor peaks in the [O II], [Ne III], and [O III] emission line profiles suggest clumping in the ejecta at velocities around $\pm$1600 km s^{-1}, and the symmetry of the emission suggests a possible ring or jet distribution. Moreover, observing minor emission peaks in the [S II] and [Ar III] profiles around $-$1600 km s^{-1} suggests that these elements are constituents of the O-rich expanding ejecta and share a similar spatial distribution.

The origin of additional minor emission peaks in the [O III] λ5007 profile around +3000 and +4600 km s^{-1} is not known. It is curious that the peaks are symmetric with the [O III] λ4959 emission line at its rest and blueshifted ($-$1600 km s^{-1}) wavelengths. Because these fainter, higher velocity peaks are not observed in the [O II] λ3727 and [Ne III] λ3869 emission lines, their reality is less certain than the stronger ones at $\pm$1600 km s^{-1}. Spectra with better S/N of the [O I], [O II], [O III], and [Ne III] lines would help investigate the possibility of additional minor emission peaks at velocities higher than 1600 km s^{-1}.

4.4. *Size and Age of the Remnant*

Although SNR 4449-1 is clearly a young object, the lack of a reported SN in NGC 4449 near the remnant's location leaves its precise age uncertain. Assuming the remnant is still in a free expansion phase despite its prodigious energy output ($\gtrsim 10^{49}$ erg across the radio, optical, and X-ray), one can obtain an age estimate from measurements of its angular size and expansion velocity.

The observed size of the remnant in the FOC F501N image is just $\approx$4 pixels (FWHM), meaning it is marginally resolved above the instrumental FWHM = 3 pixels (Fig. 26 in FOC Handbook ver. 7.0). With a 0.014″ pixel^{-1} ratio, this implies a remnant angular diameter of $\approx$0.037″, which is slightly larger than the value of 0.028″ estimated by Blair & Fesen (1998). Using the latest distance estimate to NGC 4449 of 3.82 $\pm$ 0.18 Mpc (Annibali et al. 2007), the maximum expansion velocity of 6000 km s^{-1} for [O III] implies a present age of $\sim$50 yr. This estimate is limited by both the uncertainty in the distance to NGC 4449 (between 2.93 and 5 Mpc; Karachenstsev & Drozdovsky 1998; Sandage & Tammann 1975) and the fact that the remnant is just barely resolved above the instrumental profile. However, we can conclude that the remnant is probably not much older than 100 yr, since at ages above this its size (>1.2 pc) should have been more clearly resolved in the 1996 FOC image.

Previous attempts at dating SNR 4449-1 have tried to place constraints on its age through historical plate searches to find a serendipitous detection of the associated SN outburst. De Bruyn et al. (1981) examined plates dating back to 1925 taken at Mount Wilson Observatory and found no change in the appearance of the SNR 4449-1 region. Blair et al. (1983) inspected the patrol plates of the Harvard College Observatory, including the RH series dating 1928–1954 with limiting magnitude $m_V = 14$–15 and the AC series dating 1898–1954 with $m_V = 12$. They too were unable to find any change in appearance at the location of the remnant.

We complemented the Blair et al. (1983) plate search by examining a dozen of the Harvard MC series plates from 1917 to 1954 with limiting magnitude $m_V = 17$–18 and were also unable to find any observable change in the location of the remnant. Assuming an absolute luminosity $M_V = -17$ for a typical core-collapse SN along with a $\sim$4 Mpc distance, the AC series of plates are barely within range of detection of the original SN under ideal observing conditions. And even though the MC and RH series plates are deep enough to image the original SNe, the time coverage and/or unfortunate timing of the SN outburst when NGC 4449 was behind and thus hidden by the Sun easily accounts for why these searches are inherently ambiguous and could easily miss the original supernova event.

Possibly complicating matters, earlier plate searches may have focused on the wrong time frame. Kirshner & Blair (1980) and Blair et al. (1983) estimated the age of SNR 4449-1 to be $\sim$100–200 yr using an expansion velocity of 3500 km s^{-1}. In light of recent observations, however, the velocity is really closer to 6000 km s^{-1}, implying a younger remnant with an age in line with our $\sim$50–100 yr estimation from the *HST* data. The consequence is that the prior searches, which were mostly limited to observations made previous to 1954, may have missed the original supernova if it did indeed occur later in time.

In Figure 10 we present archival images of NGC 4449 that set a minimum date for the original SNe. Figure 10*a* is a plate taken by P. Hodge in 1965 with the Lick 3 m telescope using 103aD emulsion behind a GG 11 filter (a *V*-band image), and Figure 10*b* is the same image as Figure 10*a* but zoomed in on the location of the remnant. Figure 10*c* is the 2005 ACS/WFC F555W (V) image that has been smoothed to match the resolution of the 1965 plate. The remnant is marked and stellar sources to the east and west are highlighted to show a basis of comparison. The two plate images show the SNR 4449-1 region significantly brighter in 1965 than in 2005, and we interpret this as definitively showing the remnant to be at least 42 yr old. Not presented is another plate that we examined, obtained with the same emulsion and filter combination and taken four years earlier in 1961 using the 100 inch (2.5 m) telescope at Mount Wilson. This 1961 *V*-band plate image shows the remnant just as bright, and thus further constrains the age of the remnant to be at least 46 yr.

Unfortunately, some images of NGC 4449 taken prior to 1961 cannot date the remnant with certainty. As the 1965 image illustrates, plates taken in the visual band between 5000–6000 Å are sensitive to the broad [O III] $\lambda\lambda$4959, 5007 lines and show the remnant unambiguously when compared to the recent 2005 images where we can observe a clear decline in luminosity. However, searches of older plate material using emulsions sensitive to the 3000–5000 Å wavelength region are less conclusive because the emulsions are preferentially sensitive to the UV light of the remnant's associated OB cluster.

This problem is illustrated in Figures 10*d* and 10*e*. Shown in Figure 10*d* is a plate taken on 1913 April 7 with the Mount Wilson 60 inch (1.5 m) telescope using a blue-sensitive emulsion exposed for 5 hr. Figure 10*e*, on the other hand, is the 2005 ACS/WFC F435W (B) image smoothed to match the resolution of the 1913 plate. Comparing the two, there is some drop in luminosity

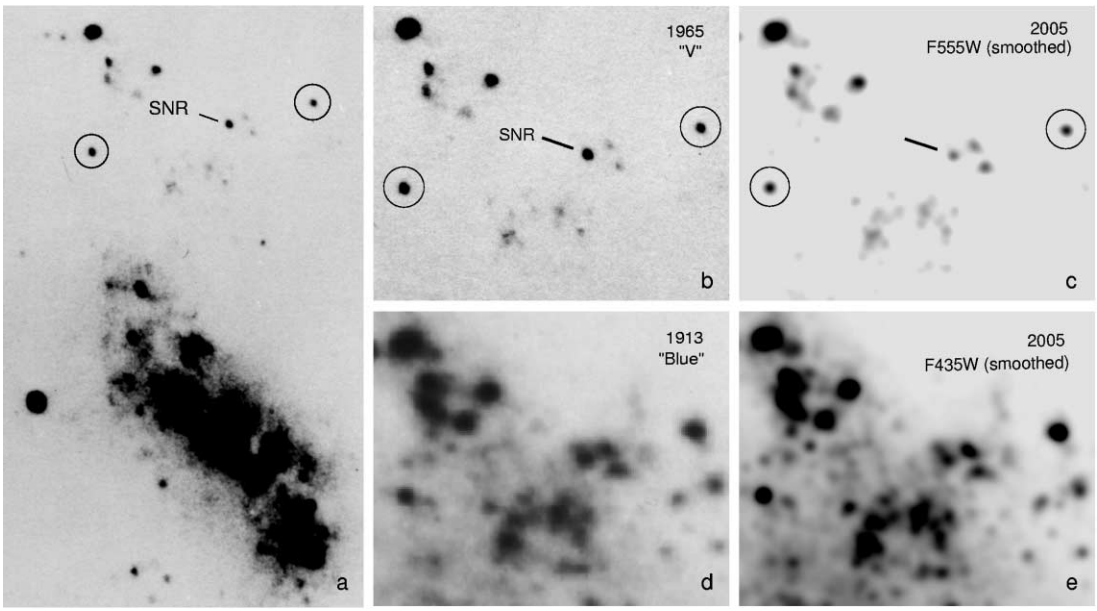

FIG. 10.—(*a*): 1965 plate of NGC 4449 taken with the Lick 3 m telescope using 103aD emulsion behind a GG 11 filter. Stellar sources are marked for brightness comparison. (*b*) The same 1965 image but enlarged around the remnant. (*c*) 2005 *HST* F555W image smoothed to match the resolution of the 1965 image. (*d*) 1913 plate taken with the Mount Wilson 60 inch telescope using blue-sensitive emulsion. (*e*) 2005 *HST* F435W image smoothed to match the 1913 image. North is up and east is to the left.

between 1913 and 2005, but nowhere near the difference observed between the *V*-band 1965 and 2005 images. We examined blue-sensitive images taken in 1917, 1935, and 1952, and the location of the remnant retained roughly the same relative brightness. Thus, while it is tempting to associate the point source located in the 1913 image with SNR 4449-1, images taken in blue-sensitive emulsion do not definitively identify the remnant because one cannot be sure whether the emission is due to the remnant or the bright, compact star cluster it is located in.

4.5. *Comparison of SNR 4449-1 with other Young SNRs and Old SNe*

SNR 4449-1's age of ~50–100 yr places it in a unique position between the youngest Galactic supernova remnants that are many hundreds of years old (Cas A being the youngest at around 325 yr; Thorstensen et al. 2001), and the eldest of extragalactic core-collapse supernovae observed a few decades after outburst. In this way SNR 4449-1 is an interesting link between SNe and their remnants, making it worthwhile to compare its properties against both types of objects.

SNR 4449-1 belongs to a small class of young O-rich SNRs. The eight known members of this SNR subclass are believed to represent the remains of high-mass stars ($\gtrsim 15\ M_{\odot}$) having debris with high velocities (>1000 km s^{-1}) and elevated abundances of oxygen and neon. Cas A is the prototypical example of this O-rich class of SNRs. Observed in Cas A are large proper motion, high radial velocity ejecta called "fast-moving knots" (FMKs; $V_{\rm exp} = 4000$–6000 km s^{-1}) that show strong O, S, and Ar lines, but no H, He, or N emissions. These knots have been interpreted as fragments of debris from the progenitor's mantle and core. Also observed are much slower moving knots called "quasi-stationary flocculi" (QSFs; $V_{\rm exp} \leq 400$ km s^{-1}) that show both hydrogen Balmer emission and strong [N II] lines consistent with them being CNO-processed CSM.

Considering SNR 4449-1 shares many optical emission properties with Cas A, they may have had similar progenitor stars. High-mass progenitor estimates of Cas A are in the range of 10–30 $M_{\odot}$ (Fabian et al. 1980; Jansen et al. 1988; Vink et al. 1998). The elevated abundances of O-burning products in Cas A's FMKs, and the slower moving He- and N-rich QSFs of circumstellar material, suggest that its progenitor may have been a WNL star that experienced substantial mass loss before exploding as a Type Ib/c or Type IIb/L SNe (Fesen & Becker 1991; García-Segura et al. 1996; Vink et al. 1996). On the other hand, lower masses between 15 and 25 $M_{\odot}$ have been suggested if instead the progenitor star interacted with a binary companion that stripped the star of its outer layers (Young et al. 2006).

If we look at SNR 4449-1 as a late-time SNe, there are very few extragalactic, core-collapse supernovae aged ≳25 yr from which to draw comparisons. Most SNe tend to fade rapidly in the optical and become nearly unobservable after 2 yr. This situation makes the high optical brightness of SNR 4449-1 in light of its age both interesting and a challenge to categorize.

The eldest and most notable examples of SNe optically recovered many years after outburst include SN 1957D (Long et al. 1989), SN 1970G (Fesen 1993), SN 1979C, and SN 1980K (Fesen et al. 1999). With the exception of SN 1957D, which was not observed near maximum, these SNe were all of Type II-L. Collectively all show high velocity (~5000 km s^{-1}) Hα, [O I] $\lambda\lambda$6300, 6364, and [O II] $\lambda\lambda$7320, 7330 emission features at late time. Yet all exhibited a flux at least ~10 times less than SNR 4449-1. It would seem that SNR 4449-1, with its much lower velocity Hα emission, greater brightness and dominating [O III] emission, may have little in common with these remnants of Type II-L.

On the other hand, SNR 4449-1 does share features in its optical spectra with two other notable recoveries of evolved SNe: SN 1986J (Leibundgut et al. 1991) and SN 1978K (Ryder et al. 1993). These SNe are both of Type IIn, a class that has been associated with dense circumstellar environments left behind by massive (possibly LBV) progenitor stars (see, e.g., Gal-Yam et al. 2007). At several years of age, SN 1986J showed intermediate-width $\Delta v \simeq 600$ km s^{-1} lines of H, He, N, and Fe, and broad $\Delta v > 1000$ km s^{-1} lines of [O I], [O II], and [O III]. Similarly, almost 20 yr after outburst, SN 1978K possessed an intermediate-width (FWHM ≤ 560 km s^{-1}) Hα profile without a high velocity base. Aside from sharing intermediate velocities, SNR 4449-1,

SN 1986J, and SN 1978K are among the rare instances where the [N II] λ5755 emission line has been observed in evolved SNe (Chu et al. 1999).

Some mention should also be made of SN 1987A, which at late time shows features in its SN ejecta-CSM interactions like those we observe in SNR 4449-1. SN 1987A was an SNe Type II-peculiar, and known to be the descendant of a 20 $M_{\odot}$ blue supergiant progenitor. Currently 20 yr past outburst, SN 1987A is interacting with circumstellar material along its equatorial ring that has, like SNR 4449-1, a high [N II] λ6583/Hα ratio and postshock density as large as $\sim 10^6$ cm^{-3} (see, e.g., Pun et al. 2002).

4.6. *Conclusion*

We have presented a collection of images and spectra, both ground based and taken by *HST*, of the young O-rich supernova remnant in NGC 4449. The nature of SNR 4449-1's bright luminosity was long suspected to be due to interaction with a surrounding H II region, but new observations suggest that the remnant is instead interacting with very dense N-rich circumstellar material from the SNR's progenitor star of mass $\gtrsim$20 $M_{\odot}$. *HST* images show that the remnant lies within a rich OB association and is located at the center of a tight grouping of bright blue stars less than a few parsecs in size.

Strong interaction of SN ejecta with a dense wind helps explain SNR 4449-1's high luminosity, and its sustained brightness suggests an extensive circumstellar environment. The advance of the forward shock through this material gives rise to the broadened Hα and [N II] emission seen, while the reverse shock from this interaction heats the O-rich expanding ejecta that dominates the presently observed optical spectrum. While we favor the scenario of the remnant running into the CSM of its own progenitor, the close proximity of the remnant to several bright stellar sources makes interaction with the wind-loss material of other stars a possibility.

We note that despite its unusual luminosity, SNR 4449-1 may represent a close match to a textbook high-mass progenitor SN scenario. That is to say, SNR 4449-1 possesses the following characteristics thought to be typical of SNe of massive stars: (1) the remnant lies within a rich cluster of high-mass stars surrounded by a presumably SN- and wind-blown ISM bubble; (2) it is located at the dense center of an OB star cluster which appears to possess some WR stars; (3) it is interacting with dense N-rich, circumstellar mass loss material; and (4) it exhibits the expected chemical properties of an H-poor envelope progenitor. Consequently, further studies of this bright SNR may help clarify the future evolution of some recent high-mass SNe which also show strong CSM interactions.

We thank John Thorstensen for obtaining the 2002 and 2006 spectra, Aaron Dotter for helping with interpretation of the photometry, Alison Doane at the Harvard College Observatory for helping us search the plate stacks, Tony Misch at Lick Observatory for helping us date plates taken by Paul Hodge, and John Grula at the Observatories of the Carnegie Institution of Washington for locating several plates of NGC 4449 taken at Mount Wilson, which Francois Schweizer helped to interpret. This research was supported in part by NSERC through a PGS award, and by NASA through grants GO-6118 and GO-10286 from the Space Telescope Science Institute, which is operated by the Association of Universities for Research in Astronomy under contract NAS 5-26555.

REFERENCES

Annibali, F., Aloisi, A., Mack, J., Tosi, M., van der Marel, R. P., Angeretti, L., Leitherer, C., & Sirianni, M. 2007, preprint (arXiv: 0708.0852)
Balick, B., & Heckman, T. 1978, ApJ, 226, L7
Blair, W. P. 1996, in IAU Colloq. 145, Supernovae and Supernova Remnants, ed. R. McCray & Z. Wang (Cambridge: Cambridge Univ. Press), 391
Blair, W. P., & Fesen, R. A. 1998, BAAS, 30, 1365
Blair, W. P., Kirshner, R. P., & Winkler, P. F., Jr. 1983, ApJ, 272, 84
Blair, W. P., Raymond, J. C., Fesen, R. A., & Gull, T. G. 1984, ApJ, 279, 708
Bowmans, D. J., Chu, Y.-H., & Hopp, U. 1997, AJ, 113, 1678
Cardelli, J. A., Clayton, G. C., & Mathis, J. S. 1989, ApJ, 345, 245
Charbonnel, C., Meynet, G., Maeder, A., Schaller, G., & Schaerer, D. 1993, A&AS, 101, 415
Chu, Y.-H., Weis, K., & Garnett, D. R. 1999, AJ, 117, 1433
de Bruyn, A. G. 1983, A&A, 119, 301
de Bruyn, A. G., Goss, W. M., & van Woerden, H. 1981, A&A, 94, L25
Dolphin, A. E. 2000, PASP, 112, 1383
Eldridge, J. J. 2006, preprint (astro-ph/0612477)
Esteban, C., Vilchez, J. M., Smith, L. J., & Clegg, R. E. S. 1992, A&A, 259, 629
Fabian, A. C., Willingale, R., Pye, J. P., Murray, S. S., & Fabbiano, G. 1980, MNRAS, 193, 175
Fagotto, F., Bressan, A., Bertelli, G., & Chiosi, C. 1994a, A&AS, 104, 365
———. 1994b, A&AS, 105, 29
Fesen, R. A. 1993, ApJ, 413, L109
Fesen, R. A., & Becker, R. H. 1991, ApJ, 371, 621
Fesen, R. A., et al. 1999, AJ, 117, 725
Ford, H. C., et al. 1998, Proc. SPIE, 3356, 234
Gal-Yam, A., et al. 2007, ApJ, 656, 372
García-Segura, G., Langer, N., & Mac Low, M.-M. 1996, A&A, 316, 133
Jansen, F., Smith, A., Bleeker, J. A. M., de Korte, P. A. J., Peacock, A., & White, N. E. 1988, ApJ, 331, 949
Karachenstsev, I. D., & Drozdovsky, I. O. 1998, A&AS, 131, 1
Kirshner, R. P., & Blair, W. P. 1980, ApJ, 236, 135
Lacey, C. K., Goss, W. M., & Mizouni, L. K. 2007, AJ, 133, 2156
Leibundgut, B., et al. 1991, ApJ, 372, 531
Long, K. S., Blair, W. P., & Krzeminski, W. 1989, ApJ, 340, L25
Lortet, M.-C. 1989, in IAU Colloq. 113, Physics of Luminous Blue Variables, ed. A. Moffatt & K. Davidson (Dordrecht: Kluwer), 45
Maeder, A., & Meynet, G. 2001, A&A, 373, 555
Massey, P., Waterhouse, E., & DeGioia-Eastwood, K. 2000, AJ, 119, 2214
O'Dell, C. R. 2004, PASP, 116, 729
Pasquali, A., Langer, N., Schmutz, W., Leitherer, C., Nota, A., Hubeny, I., & Moffat, F. J. 1997, ApJ, 478, 340
Patnaude, D. J., & Fesen, R. A. 2003, ApJ, 587, 221
Pavlovsky, C., et al. 2004, ACS Instrument Handbook, (ver. 5.0; Baltimore: STScI)
Pun, C. S. J., et al. 2002, ApJ, 572, 906
Ryder, S., et al. 1993, ApJ, 416, 167
Sabbadin, F., & Bianchini, A. 1979, PASP, 91, 280
Sandage, A., & Tammann, G. A. 1975, ApJ, 196, 313
Schneider, S. E., Thuan, T. X., Mangum, J. G., & Miller, J. 1992, ApJS, 81, 5
Seaquist, E. R., & Bignell, R. C. 1978, ApJ, 226, L5
Sirianni, M., et al. 2005, PASP, 117, 1049
Stahl, O. 1989, in Proc. IAU Colloq. 113, Physics of Luminous Blue Variables, ed. K. Davidson, A. F. Moffat, & H. J. Lamers (Dordrecht: Kluwer), 149
Summers, L. K., Stevens, I. R., Strickland, D. K., & Heckman, T. M. 2003, MNRAS, 342, 690
Thorstensen, J. R., Fesen, R. A., & van den Bergh, S. 2001, AJ, 122, 297
Vink, J., Bloemen, H., Kaastra, J. S., & Bleeker, J. A. M. 1998, A&A, 339, 201
Vink, J., Kaastra, J. S., & Bleeker, J. A. M. 1996, A&A, 307, L41
Volger, A., & Pietsch, W. 1997, A&A, 319, 459
Weaver, T. A., & Woosley, S. E. 1980, Ann. NY Acad. Sci., 336, 335
Weiler, K. W., van Dyk, S. D., Pringle, J. E., & Panagia, N. 1992, ApJ, 399, 672
Young, P. A., et al. 2006, ApJ, 640, 891